COMMENTS ON THE OPERATION OF CAPILLARY PUMPED LOOP DEVICES IN LOW GRAVITY

K. P. Hallinan[1] and J. S. Allen[2]
[1]University of Dayton, Dayton, Ohio, 45469-0210, khallina@engr.udayton.edu
[2]MS500-102,NASA-LeRC, 2100 Brookpark Rd., Cleveland, OH, 44135, jeff.allen@lerc.nasa.gov

ABSTRACT

The operation of Capillary Pumped Loops (CPL's) in low gravity has generally been unable to match ground-based performance. The reason for this poorer performance has been elusive. In order to investigate the behavior of a CPL in low-gravity, an idealized, glass CPL experiment was constructed. This experiment, known as the Capillary-driven Heat Transfer (CHT) experiment, was flown on board the Space Shuttle Columbia in July 1997 during the Microgravity Science Laboratory mission.

During the conduct of the CHT experiment an unexpected failure mode was observed. This failure mode was a result of liquid collecting and then eventually bridging the vapor return line. With the vapor return line blocked, the condensate was unable to return to the evaporator and dry-out subsequently followed. The mechanism for this collection and bridging has been associated with long wavelength instabilities of the liquid film forming in the vapor return line. Analysis has shown that vapor line blockage in present generation CPL devices is inevitable.

Additionally, previous low-gravity CPL tests have reported the presence of relatively low frequency pressure oscillations during erratic system performance. Analysis reveals that these pressure oscillations are in part a result of long wavelength instabilities present in the evaporator pores, which likewise lead to liquid bridging and vapor entrapment in the porous media. Subsequent evaporation to the trapped vapor increases the vapor pressure. Eventually the vapor pressure causes ejection of the bridged liquid. Recoil stresses depress the meniscus, the vapor pressure rapidly increases, and the heated surface cools. The process then repeats with regularity.

INTRODUCTION

Capillary pumped loops are closed loop phase change devices relying upon evaporation of liquid at the source of heat and then condensation of vapor at the sink of heat. The distinguishing characteristics of CPLs from other capillary pumped heat transfer devices are the macroscopically large vapor and liquid transport lines that ideally make possible the passive transport of heat over long distances. The porous media providing the capillary pumping is confined to the evaporator region.

The first Capillary-Pumped Loop (CPL) was developed in the 1960's at the NASA Lewis Research Center in Cleveland, Ohio (Stenger, 1966). Since then a significant number of low gravity evaluations have followed. The first of these was the Capillary Pumped Loop GAS Experiment (G-471), flown in June, 1985. The low-gravity results of this experiment are still unclear; though initial reports indicated success. The CApillary Pumped Loop (CAPL) experiment was flown in February, 1994 on board STS-60 as part of the Hitchhiker payload. This experiment tested a starter pump concept designed to clear the vapor lines of liquid prior to start-up of the CPL evaporators. Douglass (1997) reported that vapor penetrated the wick of the starter pump during operation yielding a temperature there above that of the system temperature. Further, the starter pump was never able to fully clear the vapor lines of liquid. The CAPL experiment was reflown as CAPL-2 with a redesigned starter pump in July, 1995 on board STS-69. Preliminary findings indicated performance within the thermal requirements of the EOS program (CAPL2, 1995). In November 1996, the Visualization In an Experimental Water Capillary Pumped Loop (VIEW-CPL) experiment was flown on the middeck of STS-80. This was the first experiment specifically designed to investigate the failure of CPL's in low gravity. The results of the VIEW-CPL are still preliminary, although the harmful presence of a vapor bubble within the core of the evaporator was reported (Kolos and Herold, 1997). Finally, the Two Phase Flow (TPF) experiment, designed to address problems encountered during the CAPL experiment, was flown in August, 1997 on STS-85 during the Technology, Application and Science (TAS) mission. The TPF experiment incorporated a new type of starter pump as well as a "capillary flow valve". Initial reports indicate some difficulties in start-up (Ottenstein, 1997).

In general, capillary-pumped loops have not been started from a cold state successfully without the use of a starter pump (Ku, 1995b). In most instances, the starter pump is a heated wicking structure that is used

to clear the vapor lines of liquid. Often, especially during startup, the temperature data has indicated that the liquid was flowing in reverse inside the evaporator. These experiments have also exhibited pressure oscillations accompanied by evaporator deprime (Ku and Huang, 1995a). The fundamental mechanism of the unstable operation, however, has not been identified.

The Capillary-driven Heat Transfer (CHT) experiment was designed and conducted to gain insight into the failure mechanisms of CPL devices in low gravity. The following describes the CHT experiment and the results that satisfy this objective.

EXPERIMENT

The main component of the Capillary-driven Heat Transfer (CHT) experiment is a Pyrex test loop shown schematically in Figure 1. The loops were designed to ideally model CPLs. All glass construction was used to permit observation of the fluid orientation within the whole of the CPL during testing.
Two such loops were fabricated and tested in low gravity. These loops were mounted within an enclosed experimental housing. Each was designed with an evaporator and condenser leg, having respective evaporator inner diameters of 1mm and 4mm and a 10mm inner diameter condenser. A partition wall was used to isolate these legs from each other. The vapor return line likewise had a 10mm internal diameter. The liquid return line was equal in diameter to the evaporator inner diameter. Within the loop a three-way valve was used to direct liquid (ethanol) from the 10cc reservoir into the condenser leg and/or the evaporator leg of the test loop. Conical transition sections connected the vapor leg to the capillary tubing. The conical sections were designed as capillary traps in low gravity and preferentially located the evaporator meniscus. The test fluid was spectroscopic grade ethanol.

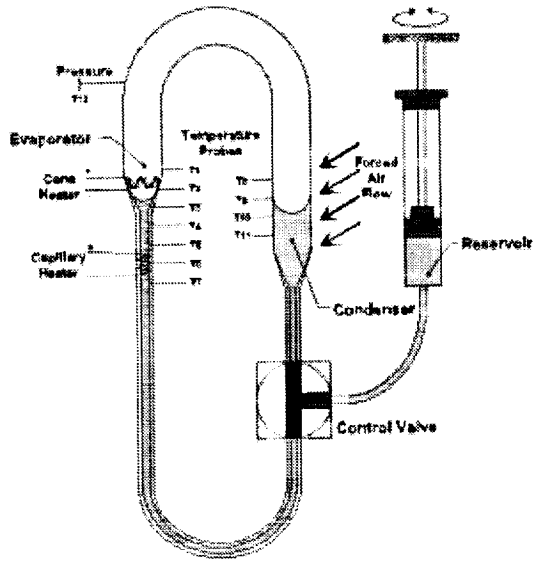

Figure 1 Schematic of experimental CPL model.

The loops were designed to prevent evaporator dry-out due to surface tension differences between the evaporator and the condenser alone even at the maximum temperature expected.

During the testing, heat could be applied to the evaporator by either of two heaters. The first, called the cone heater, was a serpentine wire attached to the evaporator conical transition section. The second, called the capillary heater, was a spiral wound wire located on the capillary tubing approximately 10 mm from the cone heater. Both heaters were constructed from 0.25mm Kanthol wire, rolled flat to insure good contact with the glass surface. A brushless fan mounted over an opening (fan vent) in the experiment module housing provided cooling for the condenser. This cooling air was exhausted through two additional openings (condenser vents) in the condenser side of the experiment module housing.

The loop was instrumented with 7 thermocouples (Type T, 40 AWG) along the length of the evaporator leg and 4 thermocouples along the length of the condenser leg. The thermocouples were located 0.25 mm from the inside wall in small diameter holes drilled into the Pyrex tubing. This proximity to the inside wall coupled with the fine gauge of the thermocouples provided a very quick response to wall temperature changes. An additional thermocouple and a pressure transducer were connected to the vapor leg to allow for a determination of the vapor properties. The loops were backlit to permit video recording of the internal phenomenon.

The output voltages from the thermocouples and pressure transducer as well as the power for the heaters and pressure transducer were fed to an LED read-out that simultaneously displayed the temperature, pressure, and heat input data. A video record of this data was obtained.

Four types of CHT experiments were conducted on the MSL-1 mission. The two relevant to the present paper were conducted as follows. In the first, liquid was added to the loop to the condenser to near the top of the straight section. Capillarity insured that the liquid in the evaporator was at the top of the evaporator conical section. Power was initiated to one of the two heaters. During the transient, evaporator meniscus stability and overall liquid orientation within the loop was observed.

The second type of experiment was referred to as the re-wetting experiments. In these, the liquid was withdrawn to the bottom of the straight section of the evaporator capillary tubing. Power was then applied to the capillary heater. After a set waiting period, the control valve was rotated to free liquid flow from the condenser to the evaporator. The subsequent re-wetting of the evaporator meniscus was then observed. Several waiting times and therefore initial temperatures were investigated.

The following sections present the results describing the dominant device failure mode - liquid slugs forming in the vapor return line that block the return of vapor to the condenser - and the related evaporator instabilities.

RESULTS

Liquid Slug Formation in the Vapor Return Lines

One of the first experimental observations was the formation of a continuous liquid film over the entire length of the vapor return leg. Immediately after applying heat, a liquid film could be seen advancing along the wall of the vapor leg on the evaporator side due to condensation of vapor on the cooler walls of the loop. Capillary forces "drain" the liquid film in the regions where the vapor tubing bends. The process of low-gravity liquid pooling in the elbow of the vapor tube and the eventual formation of a liquid slug is illustrated in Fig. 2. During each experiment run, the liquid accumulated in the outer radius of the bend in the vapor section of the test loop. This pool of liquid would collect into a lobe that would grow until a slug of liquid would form, completely bridging the vapor line.

Figures 3 and 4 show the formation of the liquid slug in the vapor leg and the subsequent recession of the condenser meniscus after the slug has formed. In Figure 3 the liquid film begins to pool in the outer radius of the bend and eventually bridges. Prior to complete bridging of the vapor line, the pooling of the liquid in the bend of the vapor leg does not adversely effect the CPL operation. However, after the liquid slug forms, condensation to the condenser meniscus is completely disrupted. Subsequently, as liquid is continually fed to the evaporator, the condenser meniscus begins to recede as shown in Figure 4. Eventually, it recedes into the capillary tube thereby eliminating the pressure difference feeding liquid into the evaporator. At this point the evaporator dries out and the system fails.

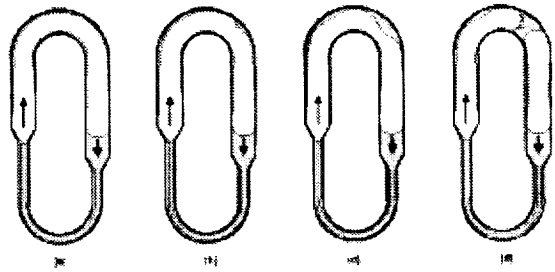

Figure 2. Illustration of liquid accumulation and slug formation in the test loop vapor leg during low-gravity CHT experiments. The arrows indicate the direction of liquid and vapor flows.

Figure 3 Formation of a liquid slug in the bend of the vapor leg.

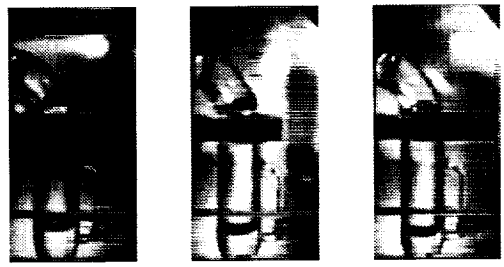

Figure 4 Recession of the condenser meniscus after formation of a liquid slug.

The formation of this slug is primarily the result of an instability arising from a long-wave disturbance of the

annular liquid film in the vapor return line. Gauglitz and Radke(1990), Aul and Olbricht (1990) and Hu and Joseph (1989) have shown that an annular film within a straight tube is fundamentally unstable to long-wave disturbances. Such a liquid film will always breakup and form periodically spaced annular lobes when the length of the liquid film exceeds a critical length. For thick liquid films, the annular liquid lobes will bridge the tube and form liquid slugs. Though this long wavelength instability is ultimately responsible for the slug formation shown in Figures 3 and 4, the liquid flow to the outer portion of the tubing bend is caused by another mechanism.

In a low Bond number (i.e., low gravity) environment, liquid in an annular film will flow from the inner to outer radius of a bend because of differences in the interfacial curvature and, therefore, liquid pressure between these two regions. These pressure differences and the liquid flow that develops are analyzed by examining four distinct regions of the annular liquid film (see Figure 5). The first region is the outer portion of the tubing bend where the liquid accumulates. Region 2 is the inside radius of the tubing bend and is located 180^0 from region 1 at the same centerline location. Regions 1 and 2 are highlighted in the cross sectional view of the annular liquid film at section A-A. Region 3 comprises the straight portion of the vapor line. Region 4 is the condenser meniscus. For the purposes of this analysis, the condenser meniscus is presumed to be far from the bend (See Allen et al., 1998, for results obtained by relaxing this requirement) and the liquid film is assumed to be of uniform thickness, h.

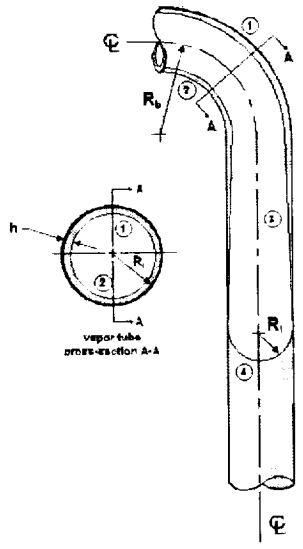

Figure 5 Geometry of the annular liquid film.

The pressure drop across a liquid-vapor interface is known from the Laplace-Young equation:

$$P_v - P_l = \sigma\left(\frac{1}{R_1} + \frac{1}{R_2}\right)$$

where P_v is the vapor pressure, P_l is the liquid pressure, R_1 and R_2 are the principal radii of curvature, and σ is the surface tension. One of the principal radii of curvature is
the same for each of the four regions and is equal to the tubing inside radius minus the film thickness, R_1 - h. The second principal radius curvature varies from region to region. In region 1 that radius of curvature is $R_b + R_1 - h$.
Similarly, $-R_b + R_1 - h$, ∞, and $R_1 - h$ are the second principal radius of curvature for regions 2, 3, and 4, respectively.

In order to simplify the analysis, a film thickness ratio is defined as $\delta = h/R$. Also, the ratio of the annular film radius to the bend radius is defined as $\Gamma = (R_1 - h)/R_b$. Substituting these and the appropriate principal radii of curvature into the Laplace-Young equation results in the following set of expressions for the pressure jump across the liquid surface for each of the four regions of the liquid film.

$P_v - P_l\|_1 = \frac{\sigma}{R_i(1-\delta)}\left(1+\frac{\Gamma}{1+\Gamma}\right)$	$P_v - P_l\|_2 = \frac{\sigma}{R_i(1-\delta)}\left(1+\frac{\Gamma}{1-\Gamma}\right)$
$P_v - P_l\|_3 = \frac{\sigma}{R_i(1-\delta)}$	$P_v - P_l\|_4 = \frac{\sigma}{R_i(1-\delta)}2$

For an isothermal system there is no vapor flow between regions 1 and 2. Likewise, for an isothermal system without significant vapor flow, the pressure drop in the vapor between each of the other regions is also assumed to be negligible. In considering a system with a condensing vapor this assumption would have to be revisited; however, in the CHT experiments before the vapor line is blocked, a majority of the condensation occurred near the condenser meniscus, so this assumption is not unreasonable. These equations are then rearranged to express the pressure drop within the annular liquid film between the various regions.

$\Delta P_l\|_{2-1} = \frac{\sigma}{R_i(1-\delta)}\left(\frac{2\Gamma}{1-\Gamma^2}\right)$	$\Delta P_l\|_{3-1} = \frac{\sigma}{R_i(1-\delta)}\left(\frac{\Gamma}{1+\Gamma}\right)$
$\Delta P_l\|_{2-3} = \frac{\sigma}{R_i(1-\delta)}\left(\frac{\Gamma}{1-\Gamma}\right)$	$\Delta P_l\|_{3-1} = \frac{\sigma}{R_i(1-\delta)}$

The potential for liquid flow can be rewritten in terms of the Capillary number. Neglecting the aspect ratio of the annular liquid film, the Capillary number is defined as $Ca = \mu U/\sigma$. Using a lubrication approximation to describe the liquid film flows, the pressure drops and

the characteristic lengths, L, between each region are combined to determine the respective velocity scales, U. The length scales and resulting capillary numbers for each of these regions are shown in Table 1.

Table 1 Length scales and Capillary numbers characterizing liquid film flows between each of the regions

Region	Length Scale	Capillary number
2-1	$\frac{\pi}{2}R_i(1-\delta)2$	$\frac{2}{\pi}\left(\frac{\delta}{1-\delta}\right)^2\left[\frac{\Gamma}{1-\Gamma^2}\right]$
3-1	$\frac{\pi}{2}R_i(1-\delta)\frac{1+\Gamma}{\Gamma}$	$\frac{2}{\pi}\left(\frac{\delta}{1-\delta}\right)^2\left[\frac{\Gamma}{1+\Gamma}\right]^2$
2-3	$\frac{\pi}{2}R_i(1-\delta)\frac{1-\Gamma}{\Gamma}$	$\frac{2}{\pi}\left(\frac{\delta}{1-\delta}\right)^2\left[\frac{\Gamma}{1-\Gamma}\right]^2$
3-4	$\frac{\pi}{2}R_i(1-\delta)$	$\frac{2}{\pi}\left(\frac{\delta}{1-\delta}\right)^2$

During the CHT experiments, the annular liquid film thickness was estimated to be 350 microns[1]. Based upon these parameters, the Capillary numbers characterizing the different regions are shown in Table 2.

Table 2 Typical Capillary numbers for the annular liquid film flow in the bend of the vapor leg during the CHT experiments.

Regions	$Ca \times 10^5$
2-1	124
3-1	20
2-3	73
3-4	361

These Capillary numbers are represented pictorially in Figure 6, where the length of the arrow is representative of the magnitude of the liquid flows. Liquid flow into the bend is much larger than the flow out of the bend. Therefore, liquid will accumulate in the outer region of the tubing bend in any low Bond number system. Also, the liquid flow into the condenser meniscus is higher than any other liquid film flows in the system. This implies that there is always significant drainage into the condenser meniscus even in low gravity systems. It also explains why the formation of the slug often took as many as 10 minutes to form. But as reported by Aul and Olbricht (1989), drainage by the meniscus will only occur over a length of $2\pi R_i$. When the condenser meniscus receded to near the conical section after a slug formed, another lobe was observed to form in region 4, since the length above the condenser meniscus to the bend approach this critical length.

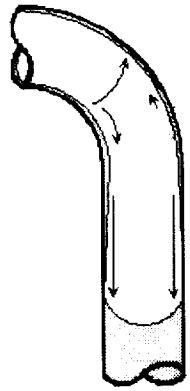

Figure 6 Vectors representing magnitude and direction of liquid film flow in CHT experiment.

The variation in the Capillary number between the various regions is a function of the geometry of the system and is not a function of the properties of the liquid (assuming constant temperature). Therefore, the liquid film flows illustrated in Figure 6 are typical of the flows in any annular liquid film within a bend in a low Bond number system where the radii ratio, Γ, is between 0.1 and 0.4. As Γdecreases below 0.1, the liquid film flow, characterized by $Ca_{2\text{-}1}$, is the dominant feature in the region of the bend, but is an order of magnitude less than the liquid flow into the condenser meniscus. At $\Gamma = 0.01$, $Ca_{2\text{-}1}$ is two orders of magnitude less than the flow into the condenser meniscus. Liquid film flows characterized by $Ca_{2\text{-}1}$ become significant relative to flows into the meniscus only when $\Gamma > 0.1$.

Characteristic Time Scales and Evaporator Meniscus Oscillations

An annular liquid film in a straight tube has been shown to be unstable when the film length exceeds a critical length of $2^{3/2}\pi R_i$ (Aul and Olbricht, 1990, Gauglitz and Radke, 1990). This long wavelength instability, driven by surface tension, results in the liquid film collecting into periodically spaced, axisymmetric "lobes". When $\delta > 0.1$ enough liquid is present that the lobes will "pinch off" and bridge the tube, forming slugs of liquid. When δ is less than 0.1, only lobes will form.

The effect of the capillary-driven flow in the bend relative to the long wavelength instability can be

[1] This estimate of the liquid film thickness is based on a uniform distribution of a volume of liquid over the entire surface of the vapor leg. The volume of liquid chosen was that which was lost from the condenser meniscus before the formation of the liquid slug

gauged through a comparison of the characteristic times for each of the flow potentials. The characteristic time associated with the long wave length instability is given by Aul and Olbricht (1989) as

$$t_\lambda = \frac{\mu_l R_i}{\sigma \delta^3},$$

where μ_l is the absolute viscosity of the liquid. This time scale characterizes the growth rate of the lobe or slug of liquid.

The circumferential flow only occurs when there is a bend in the tubing. When $\delta << 1$, the film can be treated as planar and the characteristic flow time for the circumferential flow is $\mu_l R_b / \sigma \delta^2$. For thicker films, the radial dependence of the annular film must be retained. At times during the conduct of the CHT experiment, δ exceeded 0.1, preventing use of the simpler formulation.

The radial and circumferential velocities and velocity scales in the liquid film are represented respectively by u, U and v, V. By non-dimensionalizing the radial dimension as $r = R_i(1 - \delta r^*)$, the annular liquid film thickness is scaled from 0 at the wall to 1 at the liquid-vapor interface. Applying these scales to the continuity equation yields $U \sim \delta V$. Retaining only those terms of order δ or greater reduces the conservation of momentum equations to

$$\frac{\delta^2}{R_i}\mu_l V\left(\frac{1}{1-\delta r^*}\right)\frac{\partial P}{\partial \theta} = \frac{\partial^2 v^*}{\partial r^{*2}} - \delta\left(\frac{1}{1-\delta r^*}\right)\frac{\partial v^*}{\partial r^*}$$

Using the no-slip condition at the wall and the free shear condition at the liquid surface, the dimensionless velocity profile, v^*, after eliminating terms $o(\delta)$, can be expressed as

$$v^* = \frac{\delta^2 R \Delta P_\sigma}{\pi \mu_l V}\left\{\left(r^* - \frac{1}{2}r^{*2}\right) + \delta\left(\frac{1}{2}r^{*2} - \frac{1}{3}r^{*3}\right) + \cdots\right\}.$$

Setting r^* and v^* equal to 1 results in a velocity scale equal to

$$V \sim \frac{\delta^2 R \Delta P_\sigma}{\pi \mu_l}\left(\frac{1}{2} + \frac{1}{6}\delta\right).$$

The characteristic time for the capillary flow from the inner portion of the bend to the outer portion of the bend, t_σ, is found by dividing the distance for liquid flow, πR_i, by the velocity scale, V. Substituting the expression for the capillary pressure drop from region 2 to region 1, $\Delta P_{1|2\text{-}1}$ into the velocity scale, V, results in the following expression for the characteristic time of the capillary-driven flow:

$$t_\sigma \sim \frac{\pi^2 \mu_l R_i}{\sigma \delta^2}\frac{1-\Gamma^2}{1+1/3\delta}$$

The two time scales, t_λ and t_σ, characterize the rate of liquid accumulation in the vapor line. Liquid flow in the axial direction (scaled by t_λ) will always tend to form liquid lobes whenever the film length exceeds $2^{3/2}\pi R_i$. When there is a bend in the tube, circumferential flow (scaled by t_σ) will result in liquid collecting in the outer portion of the tubing bend. ***The bend does not eliminate the long wavelength instability, but rather, it provides a perturbation to the liquid film that augments the long wavelength instability.***

The importance of t_λ relative to t_σ can be examined by expressing the time scales as a ratio,

$$t_{\lambda\sigma} = \frac{t_\lambda}{t_\sigma} \sim \frac{1}{\pi^2}\left[\frac{1+\delta^3}{\delta(1-\delta)}\right]\left(\frac{\Gamma}{1-\Gamma^2}\right)$$

The ratio of tube radius to bend radius, Γ, varies from 0 to 1. The limits on Γ vary from 0 for a straight tube to 1 for a toroid with zero inside radius. The effect of Γ on the liquid lobe formation is illustrated in Figure 7. At $\Gamma \sim 0$ (i.e., for straight tubing), $t_{\lambda\sigma} \sim 0$ and the liquid forms axisymmetric lobes. As $\Gamma \sim 1$, and $t_{\lambda\sigma} \to \infty$, a uniform liquid film forms on the outer radius of the bend. At $0 < \Gamma < 1$, $t_{\lambda\sigma} \sim 1$ and the liquid forms into non-axisymmetric lobes on the outer region of the bend. For the CHT experiments, $t_{\lambda\sigma}$ is typically around 0.4, so the formation of non-axisymmetric lobes in the bend is expected.

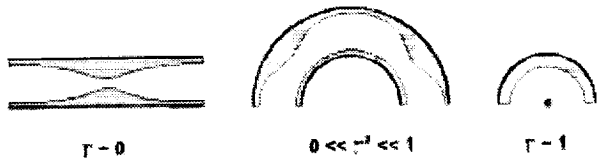

Figure 7 Types of liquid accumulation in the bend of the vapor line for various values of Γ with $\delta < 0.1$.

The ratio $t_{\lambda\sigma}$ is also a strong function of δ. The limits on $t_{\lambda\sigma}$ can be expressed in terms of the relative values of Γ and δ:

- if $\delta << \Gamma << 1$, then $t_{\lambda\sigma} \to \infty$ and the liquid film flow is characterized by t_σ;
- if $\Gamma << \delta << 1$, then $t_{\lambda\sigma} \to 0$ and the liquid film flow is characterized by t_λ.

During the CHT experiment, the liquid nearly always accumulated in the same location on the condenser side of the vapor leg. The most probable explanation for liquid accumulation in this particular location is that the radius of curvature of the bend in the glass tubing was slightly smaller at this point than at other points along the vapor leg. The non-uniform radius of curvature occurred as a result of the test loop fabrication process. The smaller radius of curvature, R_b reduces the characteristic flow time, t_λ. Therefore, liquid accumulates in the outer region of the bend more quickly at this location resulting in a larger film

thickness, δ. Since , the characteristic time for the lobe formation, t_λ, is proportional to δ^3, any small perturbation in the film thickness is greatly amplified by the long wavelength instability.

Evaporator Meniscus Oscillations

During the low-gravity CHT experiments, the evaporator meniscus did oscillate and a direct correlation of meniscus position to vapor pressure was established. Portions of two CHT rewetting experiment runs are provided which illustrate this relationship.

Figure 8 shows a small time segment (12 seconds) taken from the first rewetting experiment run,near the beginning of the test run when the system was far from steady-state. In Fig. 8 the upper graph shows the evaporator wall temperatures TC5 and TC6 against time. The major time divisions are in 30 frame (1 second) increments. TC6 is located in the center of the capillary heater and TC5 is located just beyond the capillary heater towards the vapor side of the loop. The center graph is a plot of the vapor pressure versus time. The lower graph plots the evaporator meniscus position against time. The meniscus position is referenced from thermocouple 3. The horizontal grid lines on the bottom graph are the locations of thermocouples 1 through 7.

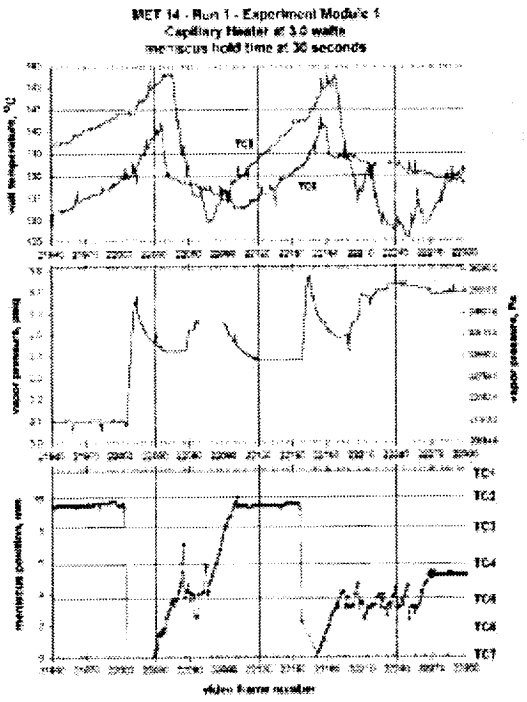

Figure 8 Time slice of evaporator wall temperatures, vapor pressure, and evaporator meniscus position from the CHT rewetting experiment - run 1.

In Figure 8 the meniscus was stable and located near TC 2 until frame 22000. Complete rewetting had occurred. Then the meniscus violently destabilized. Vapor recoil depressed the meniscus below thermocouple 7. Simultaneously, the vapor pressure jumped 4000 Pa, and after a one second time lag the wall temperatures TC6 and TC5 began to drop. These two temperatures begin to decline again once the meniscus began to move back into the evaporator.

After another 100 frames, the evaporator meniscus restabilized near TC2. Once the meniscus stabilized, the vapor pressure begins to drop, eventually leveling off, and the wall temperatures began to rise. At frame 22156, the process repeated. In all cases, the vapor pressure spikes were directly attributable to the destabilization of the evaporator meniscus (characterized by a dramatic and rapid recession).

Figure 9 shows a 12 second time slice from the second rewetting experiment run, taken near the end of the test run where quasi-steady-state operation is being approached. At the beginning of this time slice, the evaporator meniscus was oscillating with a very small amplitude (~ 500 microns) near the TC5 location. The frequency of these oscillations were about 6 to 10 Hz. The small oscillations produced vapor pressure changes that could not be resolved by the pressure transducer. At frame number 7542, the evaporator meniscus suddenly stabilized and advanced to the TC2 location. Simultaneously, the vapor pressure began to drop as the evaporation was reduced and the wall temperatures increased, especially at TC5. After 1.2 seconds (frame 7578) the meniscus violently destabilized and once again began to oscillate about the TC5 location. As the evaporation increased the vapor pressure also increased and the wall temperature at TC5 decreased dramatically. This cycle is repeated again starting at frame 7680.

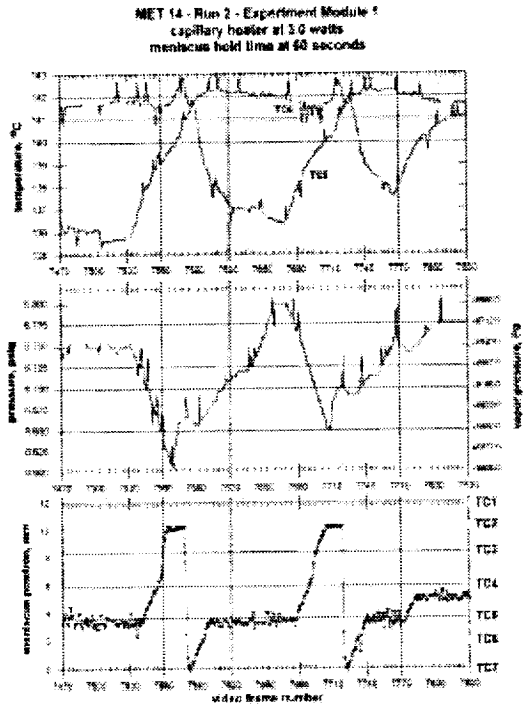

Figure 9 Time slice of evaporator wall temperatures, vapor pressure, and evaporator meniscus position from the CHT rewetting experiment - run 2.

That there is a periodic nature to these oscillations is obvious from the power spectrum analysis of the temperature data for TC7 (near the normal position of the meniscus) during run 2 for the period of time when the meniscus oscillations were present. See Figure 10. Clearly, a significant portion of the signal energy is in the 7 Hz range.

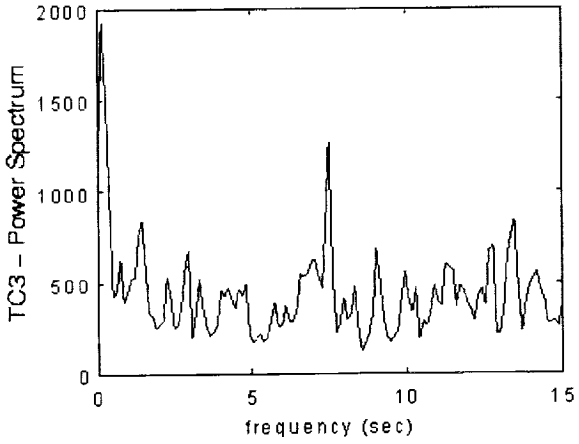

Figure 10 Power spectrum analysis of TC7 during second rewetting experiment

The previous results establish the link between vapor pressure oscillations and the meniscus destabilization and show that these oscillations are periodic. However, these do not reveal their source. One potential mechanism can be eliminated from consideration. Nucleate boiling was not observed in any of the tests.

For some of these oscillations, a liquid bridge was observed to form upstream of the intrinsic meniscus in the capillary tube. When this occurs, evaporation to the entrapped vapor bubble increases the pressure within. Eventually the liquid bridge is ejected. Given that the length in the capillary tube above the intrinsic meniscus was greater than $2^{3/2}\pi R_e$, where R_e is the internal radius of the evaporator capillary, the possibility of a long wavelength instability could not be ignored.

To see if the characteristic frequency of the observed oscillations can be explained by this mechanism, the time scale, t_λ for the formation, growth, and coalescence of lobes in the evaporator capillary is determined. To accomplish this, an estimate for the dimensionless film thickness, δ, is required. Generally, in ground tests, the initial lobe and slug formation was slowest. After the first incidence, however, the observed rate of formation increased rapidly, suggesting that much of the liquid ejected from the liquid bridge when the vapor pressure becomes sufficient to blow through the liquid bridge, finds its way to the wall of the capillary. The initial liquid film thickness after ejection of the bridge can then be estimated from the volume in the liquid bridge. Presuming the bridge volume to be roughly equal to one half of the cross-sectional area of the evaporator capillary times the critical length, ($\pi^2 R_e^3 2^{1/2}$), the dimensionless liquid film thickness after ejection of the bridge can be estimated as:

$$\delta \sim h/R_e = 2^{-1/2}\pi R_e/L$$

where L is the length of the evaporator capillary length above the bridge (~ 1 cm). This dimensionless film thickness is estimated to be 0.11, suggesting that liquid bridging is likely (Aul and Olbricht, 1990).

Now, the time scale t_λ is estimated. Evaluating the thermophysical properties at TC7, the time scale for lobe formation and bridging is on the order of 0.08s. Since this period is less than that associated with the oscillations, the possibility that the long wave instability contributes to their occurrence cannot be discounted. Further, since the time scale is very small, the absence of visual observation of liquid bridging prior to the meniscus oscillations for every occurrence may be a consequence of aliasing introduced by the 1/30 second video recording rate.

CONCLUSIONS

The CHT experiment has provided significant insight into of the fundamental operation of a capillary pumped loop heat transfer device in low-gravity. Above all, it has revealed that the present criteria used to design such systems which ignores the presence of liquid in the so-called adiabatic vapor transport region and that ignores the dynamics within the evaporator pores is inadequate for low-gravity systems. The present research has shown that the liquid film forming along the walls of the *adiabatic* region will inevitably de-stabilize due to a long wavelength instability mechanism, particularly given the long transport lines characteristic of CPL's. The present research has further shown that bends in these lines will amplify the long wavelength disturbances due to the accumulation of liquid at the outer radius of the bend due to capillary pumping. Given that CPL's rely have multi-pass heat exchangers comprising the condensers, the significance of this result is clear. In time, a liquid slug will form in each and every bend. With this conclusion, the past low gravity CPL results must be looked at with some suspicion. A majority of these tests have focused on CPL start-ups. The present results yield uncertainty about whether steady-state CPL operation is obtainable at all.

The present research has also offered a plausible explanation for the vapor pressure oscillations that have been observed in CPL's in the past. Analysis reveals that long wavelength instabilities present in the evaporator pores can lead to liquid bridging and vapor entrapment in the porous media. Subsequent evaporation to the trapped vapor increases the vapor pressure. Eventually the vapor pressure causes ejection of the bridged liquid. Recoil stresses dramatically depress the meniscus. As the meniscus attempts to rewet, the process then repeats. At high enough temperatures, wetting degradation is observed to coincide with these cyclic oscillations.

ACKNOWLDGEMENTS

We would like to acknowledge the support of NASA Microgravity Sciences Directorate under grant number UGS96-0038.

REFERENCES

Allen, J. S., Hallinan, K. P., and Lekan, J., " A Study of the Fundamental Operations of a Capillary Driven Heat Transfer Device in Both Normal and Low Gravity," presented at the 1998 STAIF Conference, Albuquerque, NM, January 27-29.

Aul, R.W. and Olbricht, W.L., 1990, "Stability of a Thin Annular Film in Pressure-Driven, Low-Reynolds Number Flow Through a Capillary," *J. of Fluid Mechanics*, 215, pp. 585-599.

Butler, D., 1986, "The Capillary Pumped Loop (CPL) GAS Experiment, G-471," Post Flight Data Report.

CAPL-2 Experiment Team, 1995, CAPL-2 Final Mission Status Report, Posted by the Goddard Space Flight Center -- Thermal Engineering Group at World Wide Web site http://sspp.gsfc.nasa.gov/capldata.html.

Douglas, D. and Ku, J. and Schlager, L., 1997, "Investigation of the Starter Pump Purge Superheat Observed in the CAPL 1 Flight," AIAA 97-3871, presented at the 1997 National Heat Transfer Conference, Baltimore, Maryland.

Gauglitz, P.A. and Radke, C.J., 1990, The Dynamics of Liquid Film Breakup in Constricted Cylindrical Capillaries,
Journal of Colloid and Interface Science, 134, No. 1, pp. 14-40.

Hu, H. H. and Joseph, D. D., 1989, "Lubricating Pipelining: Stability of Core-Annular Flow. Part 2," *Journal of Fluid Mechanics*, 205, pp. 359-396.

Kolos, K. R. and Herold, K. E., "Low Frequency Temperature and Fluid Oscillations in Capillary Pumped Loops," AIAA 97-3872, Presented at the 1997 National Heat Transfer Conference, Baltimore, Maryland.

Ku, J. and Hoang, T., 1995a, "An Experimental Study of Pressure Oscillation and Hydrodynamic Stability in a Capillary Pumped Loop," Presented at the 1995 National Heat Transfer Conference, Portland, Oregon.

Ku, J., "Start-up Issues in Capillary Pumped Loops," Presented at the 9th International Heat Pipe Conference, Albuquerque, New Mexico.

Ottenstein, L., 1997,"Two-Phase Flow Post Mission Briefing," Presentation Handout.

Stenger, F. J., "Experimental Feasibility Study of Water-Filled Capillary-Pumped Heat Transfer Loops," NASA Lewis Research Center, Cleveland, Ohio, NASA TM X-1310.